Applied Thermal Engineering 248 (2024) 123334

Contents lists available at ScienceDirect

Applied Thermal Engineering

journal homepage: www.elsevier.com/locate/apthermeng

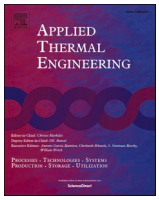

Research Paper

Flow and heat transfer characteristics of torsional tube cluster heater in a Stirling engine

Feng Xin [a,b], Kai Yang [a], Bin Zhao [a], Yanfeng Yang [a], Wei Liu [b,*], Zhichun Liu [b,*]

[a] School of Energy and Power Engineering, Changsha University of Science and Technology, Changsha 410114, China
[b] School of Energy and Power Engineering, Huazhong University of Science and Technology, Wuhan 430074, China

ARTICLE INFO

Keywords:
Heat transfer performance
Heating tube
Torsional tuber cluster
U-shaped tuber cluster
Stirling engine

ABSTRACT

The heater in a Stirling engine is a component connecting external heat source and internal working medium. Enhancing the heat transfer of the heater is key to improve the actual efficiency of the Stirling engine. Currently, tubular heaters are the most commonly used heat exchangers, and their tube clusters are primarily arranged in a U-shaped. In this study, the heat transfer performance of a novel torsional tube cluster heater was investigated using numerical simulations. The temperature, pressure, and velocity cloud patterns were analysed. The results indicated that the lateral scouring velocity component of the external flue gas was generated using the torsional tube cluster heater without altering the heating chamber volume, thereby prolonging the heating time and flow path of the working medium. The temperature of the outlet working medium was increased by 53 K by using a torsional tube cluster heater, thereby enhancing the work power of the working medium entering the expansion chamber. In addition, the torsional tube cluster heater displayed broad applicability to different working medium types for heat transfer enhancement. This study provides a feasible strategy to improve the practical operation efficiency of a Stirling engine from the perspective of tube cluster optimization of the heater.

1. Introduction

Stirling engines are external combustion engines that can use traditional and renewable energy. Stirling engines also have the advantages of high theoretical efficiency, simple structure, and low noise [1–3]. Therefore, they have been widely used in the fields of waste heat recovery [4,5], underwater power [6], space power [7,8], and micro-combined heat and power [9,10]. A Stirling engine consists of an expansion chamber, a compression chamber, a heater, a regenerator, and a cooler. The thermal expansion and cooling compression of the working medium are the intrinsic driving power of the external work. The temperature difference between the heat source and the working medium for the heater significantly exceeded that between the cold source and the working medium for the cooler. Therefore, the enhancement of heat transfer in the heater is vital for increasing the practical operation efficiency of Stirling engines [11,12].

Stirling engine heaters are typically classified into finned and tubular types. Heaters with different types of fins are commonly used for low-power Stirling engines below 100-watt level owing to their simple structure and small heat exchange capacity [13–16], whereas the tubular heaters with large heat exchange capacities are widely used in various Stirling engines[5,17,18]. The general strategy for enhancing the heat transfer of tubular heaters is to optimize the geometric parameters of the heater, such as tube length, inner tube diameter, and tube amount [19–21]. The empirical correlation of heat transfer in a heater can be built by studying the heat transfer and pressure drop under different geometric parameters, which can be adopted to guide the Stirling engine heater design [22]. Additionally, the effects of the geometric structure of different assembly units, including heating tubes, cooling tubes, and regenerators, on the thermal efficiency, output power, and flow resistance losses can be investigated synergistically [23]. This strategy can optimize the geometric structure of the heat from the perspective of maximising the overall performance of the Striling engine. Although the heat-transfer performance can be improved by optimising the geometric structure of the heater, the size of the heating chamber generally increases, thus affecting the structural compactness of the Stirling engine.

The application of various types of spoilers has been demonstrated to be effective in improving the heat transfer performance of heat exchangers [24–26]. Such strategies for heat transfer enhancement have been widely applied in conventional flow, whereas the applications under the conditions of the heat exchanger in a Stirling engine are still limited. These studies have shown that heat transfer enhancement

* Corresponding authors.
E-mail addresses: w_liu@hust.edu.cn (W. Liu), zcliu@hust.edu.cn (Z. Liu).

https://doi.org/10.1016/j.applthermaleng.2024.123334
Received 22 January 2024; Received in revised form 15 April 2024; Accepted 1 May 2024
Available online 3 May 2024

Nomenclature

C_1	constant number
C_2	constant number
C_3	constant number
c_p	specific heat ($J{\cdot}kg^{-1}{\cdot}K^{-1}$)
d	expansion chamber diameter(mm)
d_i	inner diameter of heating tube (mm)
d_o	outer diameter of heating tube (mm)
D	heating chamber inside diameter(mm)
G_b	turbulence kinetic energy due to buoyancy ($J{\cdot}kg^{-1}$)
G_k	turbulence kinetic energy due to velocity gradient ($J{\cdot}kg^{-1}$)
h	heat transfer coefficient($W{\cdot}m^{-2}{\cdot}K^{-1}$) expansion chamber height(mm)
H	heating chamber height(mm)
k	thermal conductivity ($W{\cdot}m^{-1}{\cdot}k^{-1}$) turbulent kinetic energy ($J{\cdot}kg$)
l_1	length of outer tube (mm)
l_2	length of inner tube (mm)
P	pressure (Pa)
r_n	distance between tube outlet and heater center(mm)
r_w	distance between tube inlet and heater center(mm)
R	bend radius of tube(mm)
S_T	viscous dissipation($W{\cdot}m^{-2}$)
S_E	the heat of solid (J)
t	ime (s)
T	temperature (K)
u	velocity ($m{\cdot}s^{-1}$)
Y_M	fluctuating dilatation

Greek symbols

α	circumferential torsional angle of outer tube(°)
β	circumferential torsional angle of inner tube(°)
δ	expansion chamber wall thickness(mm)
λ	thermal conductivity ($W{\cdot}m^{-1}{\cdot}k^{-1}$)
ε	dissipation rate($m^2{\cdot}s^{-2}$)
μ	viscosity ($kg{\cdot}m^{-1}{\cdot}s^{-1}$)
μ_t	turbulent dynamic viscosity ($kg{\cdot}m^{-1}{\cdot}s^{-1}$)
ν	dynamic viscosity($m^2{\cdot}s^{-1}$)
ρ	density ($kg{\cdot}m^{-3}$)

subscripts

i,j	coordinate directions
k	turbulent kinetic energy ($J{\cdot}kg$)
ε	dissipation rate($m^2{\cdot}s^{-2}$)

significantly depends on the spoiler structure. The spoiler can be placed either outside or inside the heating tube of a Stirling engine. For instance, the velocity distribution of the heat source gas was changed using guide and diffuser plates outside the heating tube cluster surface, thereby enhancing heat transfer performance [27]. The convective and radiative heat transfer of the heater can be changed by adding steel wool between the tube cluster and the heating chamber [12], in which secondary and rotating flows were generated to significantly increase the comprehensive heat transfer coefficient of the heater. The application of circular, pin, or rectangular fins inside the heater is also an effective way to enhance the heat transfer performance [13]. Additionally, inserting a spiral coil inside the heating tube or adopting a spiral-corrugated tube can generate a spiral flow field and extend the flow path of the fluid, thereby enhancing the heat transfer performance of the heater [11,28]. These methods can sufficiently disturb the flow field and thus enhance the heat transfer performance; nevertheless, they are usually accompanied by significant resistance loss.

New technologies must be developed for heat transfer enhancement in Stirling engines that neither increase the heater tube volume nor turbulence resistance significantly. From this perspective, changing the arrangement of the heater tube clusters may be an effective approach. The heating tube clusters are generally arranged as straight type [22,29–32] and U-shaped [17,21,33–35]. The straight type consists of several identical straight tubes arranged at equal spacing. The heat transfer performance is significantly affected by the tube arrangement, such as circular, square, or staggered [22,30]. For instance, the arrangement of straight tubes in a square formation was more effective than other tube arrangement for a solar Stirling engine heater when adopted in a micro-cogeneration system [31]. Nevertheless, there are also some research findings showing that a circular arrangement is the most effective configuration under specific geometrical parameters compared to square and staggered arrangements [22]. Although optimizing the arrangement of the straight-type heating-tube clusters enhanced the heat-transfer performance of the heater to a certain extent, the regenerator and expansion chamber were connected to both ends of the straight heating tube, resulting in a large space occupying to cause a large volume of Stirling engine.

Compared to the straight-type tube clusters, the U-shaped tube clusters have been widely adopted in Stirling engines owing to their high space utilization. The working medium was arranged inside the heating tube, and the heat source was arranged outside the heating tube, in which the middle part of the heating tube was bent into a U-shape [9,36–38]. The operation condition and working medium characteristics significantly affected the heat transfer of the U-shaped tube cluster heater (denoted as UTH) [39]. Xiao et al. [40] investigated the effects of heating power, oscillatory frequency, and gas pressure on the heat transfer characteristics of a U-shaped tube cluster heater, in which an increase in gas pressure was favorable for enhancing the heat transfer of a U-shaped tube cluster heater. Ni et al. [41] studied the type of working medium (i.e., helium, carbon dioxide, and nitrogen) on the heat transfer characteristics of a U-shaped tube cluster heater. The results indicated that the heat transfer coefficients of carbon dioxide and nitrogen were slightly lower than those of helium. These studies were primarily conducted by building empirical heat transfer correlations, which can be adopted to forecast the heat transfer performance of a U-shaped tube cluster heater.

In summary, most of the current studies on UTH have focused on the effect of the operating conditions and working medium characteristics on the heat transfer performance of the heater. There has been a lack of exploration into further optimization of the structure and arrangement of U-shaped tube cluster heaters. An excellent tube cluster arrangement structure is crucial for improving the performance of Stirling engine heaters. Heaters with U-shaped tube cluster arrangements capture the maximum marked share and are widely used in various fields. The tube cluster arrangement structure improves heat transfer and reduces energy loss, which might benefit all of them. In addition, compactness is a critical factor in determining the wide application of Stirling engines in various fields, such as aerospace and submarines. The important goal for the tube cluster structure optimization of the heater is heat transfer enhancement, while its space ratio should not be ignored, and it is best not to add to its size. Therefore, if there is a more efficient tube cluster arrangement than the U-shaped tube cluster, which could enhance the heat transfer without compromising the compactness, or reduce the heating chamber volume without affecting the heat transfer, the comprehensive performance of the Stirling engine would be improved, and its application would be more promising.

From these perspectives, this study aims to design a novel torsional tube cluster heater (i.e. a torsional tube cluster heater) to enhance the

heat transfer performance without compromising its compactness compared to the conventional UTH. This study was conducted using three-dimensional numerical simulation methods. First, the velocity, temperature and pressure fields in a torsional tube cluster heater were investigated to explore the heat transfer enhancement mechanism. Second, the influences of the torsional geometric parameters and fluid operating parameters on the exit temperature of the working medium in the heater tube (i.e., the inlet temperature of the working medium in the expansion chamber) were studied. Finally, the heat transfer enhancement capacity of the torsional tube cluster heater is investigated using different types of working media. The goal of this study is to increase the heater outlet temperature under the same external heat source and heater inlet conditions, thereby improving the working ability of the working medium in the expansion chamber of the Stirling engine.

2. Physical and mathematical models

2.1. Physical model

Fig. 1 shows a schematic diagram of the Stirling engine heater. The tube clusters were placed in a cylindrical heating chamber. The heat source was a high-temperature flue gas from natural gas. The flue gas flowed downwards from the top of the heating chamber. The heat released during the process was absorbed by the heating tube cluster. The heating system comprised of 26 tubes, where the inlet end was connected to a regenerator and the outlet end was linked to an expansion chamber. The working medium in the heating tubes was heated by the flue gas when it passed through the heater. This study compared the performance of two types of heater tube clusters: a conventional UTH and a novel torsional tube cluster heater (TTH). The single heating tube of the TTH included two connected torsional sections, where the outer perimeter l_1 corresponds to the torsion angle α and the inner perimeter l_2 corresponds to the torsion angle β. Structure diagrams of the two types of heater tube clusters are presented in Fig. 1 (a) and Fig. 1 (b). The geometric parameters of the UTH in this study are largely inspired by the literature [42]. The TTH has the same parameters as UTH except for the shape of the heating tubes. The geometric parameters of the heater are listed in Table 1.

2.2. Mathematical modelling

2.2.1. Control equations

The flow inside the heater was assumed to be compressible, turbulent, and non-isothermal. The control equations are as follows:

Continuity equation:

$$\frac{\partial \rho}{\partial t}+\nabla\cdot(\rho\vec{u})=0 \tag{1}$$

where the $\vec{u}$ denotes the velocity vector.

Momentum conservation equation:

$$\frac{\partial(\rho\vec{u})}{\partial t}+\nabla\vec{u}\cdot(\rho\vec{u}) = -\nabla P-\frac{2}{3}\nabla[\mu(\nabla\cdot\vec{u})]+\nabla\cdot[\mu(\nabla\cdot\vec{u})^{T}]+\nabla\cdot[\mu(\nabla\vec{u})] \tag{2}$$

Energy conservation equations:

$$\frac{\partial(\rho T)}{\partial t}+\nabla\cdot(\rho\vec{u}T)=\nabla\cdot(\frac{k}{c_p}\mathrm{grad}T)+S_T \tag{3}$$

where S_T denotes the thermal energy converted from the mechanical energy owing the viscous effect.

k-ε turbulence equation:

$$\frac{\partial}{\partial t}(\rho k)+\frac{\partial}{\partial x_i}\left(\rho k\vec{u}_i\right)=\frac{\partial}{\partial x_j}\left[\left(\mu+\frac{\mu_t}{\sigma_k}\right)\frac{\partial k}{\partial x_j}\right]+G_k+G_b-\rho\varepsilon-Y_M \tag{4}$$

$$\frac{\partial}{\partial t}(\rho\varepsilon)+\frac{\partial}{\partial x_i}\left(\rho\varepsilon\vec{u}_i\right)=\frac{\partial}{\partial x_j}\left[\left(\mu+\frac{\mu_t}{\sigma_\varepsilon}\right)\frac{\partial\varepsilon}{\partial x_j}\right]+\rho C_1S_\varepsilon-\rho C_2\frac{\varepsilon^2}{k+\sqrt{\nu\varepsilon}}+C_{1\varepsilon}\frac{\varepsilon}{k}(C_{3\varepsilon}G_b) \tag{5}$$

where

$$C_1=\max\left[0.43,\frac{\eta}{\eta+5}\right],\ \eta=S\frac{k}{\varepsilon},\ S=\sqrt{2S_{ij}S_{ij}} \tag{6}$$

where S_{ij} is the strain rate tensor, G_k is the generation of turbulence kinetic energy due to mean velocity gradients, G_b is the generation of turbulence kinetic energy due to buoyancy, Y_M is the contribution of the

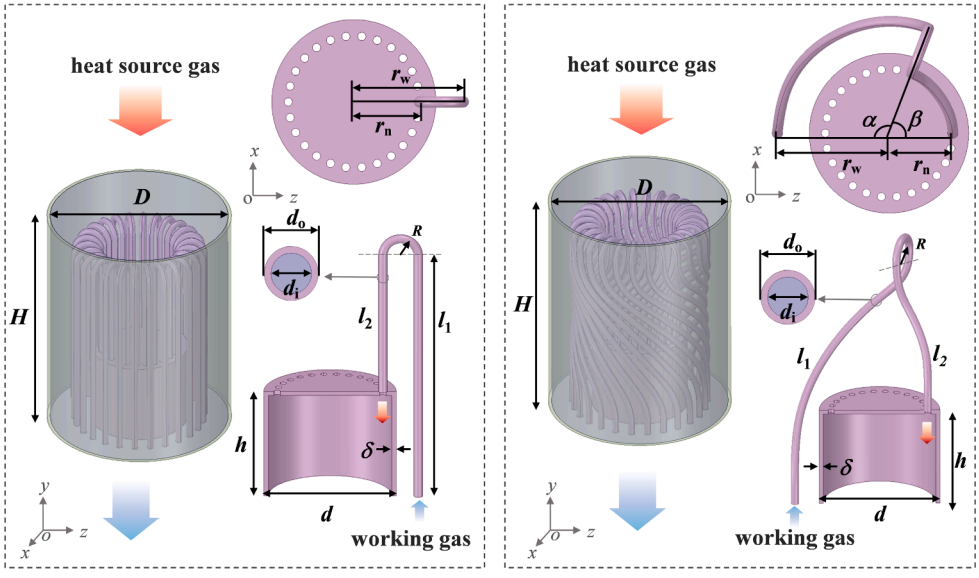

Fig. 1. Structure diagram of the Stirling engine heater: (a) UTH; (b) TTH.

Table 1
Specific geometric parameters of the Stirling engine heater Unit: mm.

Heater type	D	H	d	h	r_w	r_n	R	d_i	d_o	δ	α/°	β/°	l_1	l_2
UTH	110	142	60	50	42	26	9	3	4	2	0	0	115	65
TTH	110	142	60	50	42	26	9	3	4	2	40–150	30–80	124–168	71–80

fluctuating dilatation incompressible turbulence to the overall dissipation rate. σ_k, σ_ε, $C_{1\varepsilon}$, $C_{2\varepsilon}$, and $C_{3\varepsilon}$ are the model constants used to calibrate based on different flow types, such as shear flows and homogeneous flows.

Thermal conductivity equation for solid domain:

$$\frac{\partial(\rho c_p T)}{\partial t} = \nabla\cdot(\lambda\nabla T) + S_E \tag{7}$$

A more detailed explanation of each symbol in the above formulas is provided in the literatures [11,18,42].

2.2.2. Boundary conditions

The boundary conditions for the numerical simulation were determined by theoretical calculations based on a Stirling engine, including fuel combustion calculations (i.e., natural gas combustion), and each part of the heat transfer calculation (i.e., the heat transfer between the flue gas and tube outer wall, heat conduction of the tube wall, and heat transfer between the inner tube wall and working medium). The boundary condition values were first assumed and then they were tested by calculating the heat balance, where the heat released from the combustion of natural gas was equal to the heat absorbed by the heater and flue gas. Iterative calculations were conducted until the deviation between the assumed and calculated values was less than 5 %. Subsequently, the values of the boundary conditions are determined. The basic parameters of the Stirling engine and the final boundary conditions applied in the numerical simulation were as follows:

The operation parameters of the Stirling engine, which was designed for use in a micro-cogeneration system, were as follows: rated output power of 1000 W, natural gas as fuel, helium as the working medium (as well as hydrogen, nitrogen, air, argon, and carbon dioxide as the contrasting working medium in our study (see Section 3.4.3)), average pressure of 2.0 MPa, piston diameter of 56 mm, piston stroke of 25 mm, rotational speed of 1500 r/min, and frequency of 25 Hz.

The boundary conditions used in this study included three parts. Their types and setting values were as follows: (i) Flue gas side: the inlet was set as the velocity boundary condition, the velocity was set to 1–5 m/s, and the temperature was set to 1647 K. The outlet was set as the pressure boundary condition, and the pressure was set to 0 Pa. The cylindrical heating chamber wall was set as an adiabatic wall. (ii) Working medium side: The inlet was set as the velocity boundary condition, the velocity was set to 5–25 m/s, and the temperature was set to 600 K. The outlet was set as the pressure boundary condition, and the pressure was set to 2 MPa. The cylindrical heating-chamber wall was set as an adiabatic wall. (iii) Tube wall: The contact regions between the solid and fluid domains (inner and outer wall surfaces of the heating tube) were associated together using the Ansys meshing. The interfaces were automatically generated for the coupling of the solid/fluid heat transfer when the mesh was imported into Fluent.

2.2.3. Other setting information about numerical simulation

The finite volume method was used to compute the flow through the heater. The numerical simulation used a coupled flow-solid calculation model. The SIMPLE algorithm was employed to couple the pressure and velocity using a separation solver for the pressure basis. To select a suitable turbulence model, the studies with different turbulence models (standard k-ε model, RNG k-ε model, realizable k-ε model, standard k-ω model, SST k-ω model) were conducted for a tube cluster heater, and the results were compared with the study in literature [34]. The results show that the numerical simulation using a realizable k-ε model could be achieve the best accuracy with relatively few iteration steps, which was selected for this study. The detailed comparison results are shown in Fig. 2. During the numerical simulation, the convergence was considered to be achieved when the energy equation was below 10^{-6}, and the other equations were below 10^{-4}.

2.3. Reliability verification

2.3.1. Grid independence verification

Grid-independence validation was performed prior to the calculations. The calculation zone for TTH was divided into six sets of grids ranging from 9.2 to 19.4 million. The inlet velocities of the flue gas and working medium were set to 3 and 15 m/s, respectively. As shown in Fig. 3, increasing the grid number from 14.96 million to 17.6 million only led to a change of less than 0.02 % in the working-medium temperature at the heater tube outlet. Thus, to balance calculation time and accuracy, a grid number of approximately 15 million was adopted for subsequent calculations.

2.3.2. Model validation

To verify the validity of the model, the numerical simulation results in this study were compared with experimental [43] and simulation results [34] in the literatures. For the former, the study object was a U-shaped heater cluster (similar to the UTH in this study), whose geometric model is shown in Fig. S1(a) in the Appendix. The detailed geometric and operating parameters during the simulation are based on experimental information in the literature [43], which are described in the Appendix . Fig. 4 (a) shows the output power of the Stirling engine at three different heating temperatures. The error between the numerical simulation results and the experimental results was in the range of 1.2–5.6 %. For the latter, the study object was similar to a U-shaped heating tube cluster but more similar to a V-shape in the turn-back bend part. The geometric model is shown in Fig. S1 (b) in the Appendix . The detailed geometric and operating parameters during the simulation were based on the data in the literature [34], which are described in the Appendix . Fig. 4 (b) shows the temperature distribution of the work medium at various locations in the heating tube at a phase angle of 180°. The temperature distribution and spatial variation in the numerical simulation were consistent with results in the literature, with errors

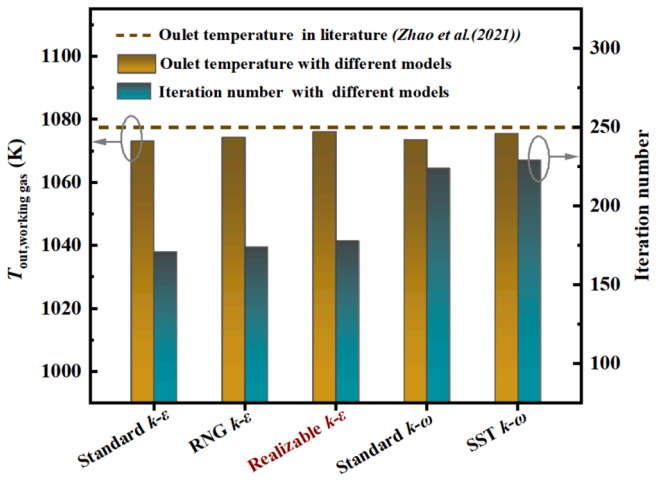

Fig. 2. Comparison and selection of turbulence models.

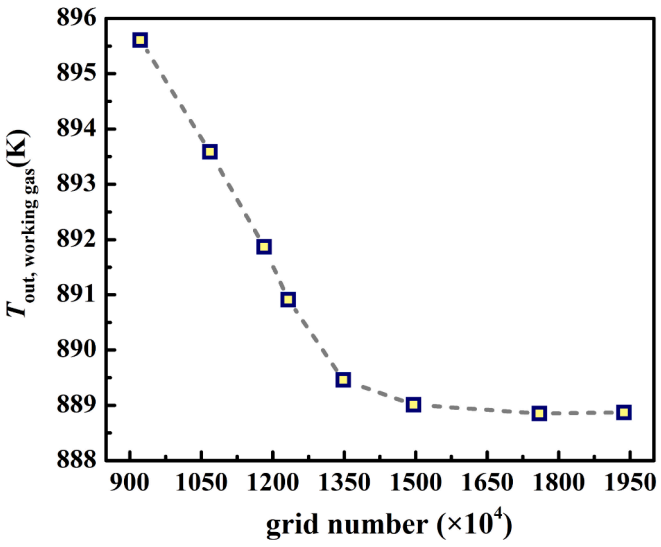

Fig. 3. Grid independence verification of the heater.

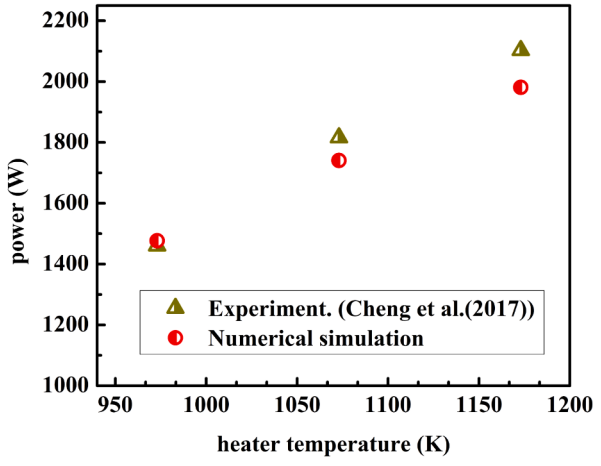

(a)

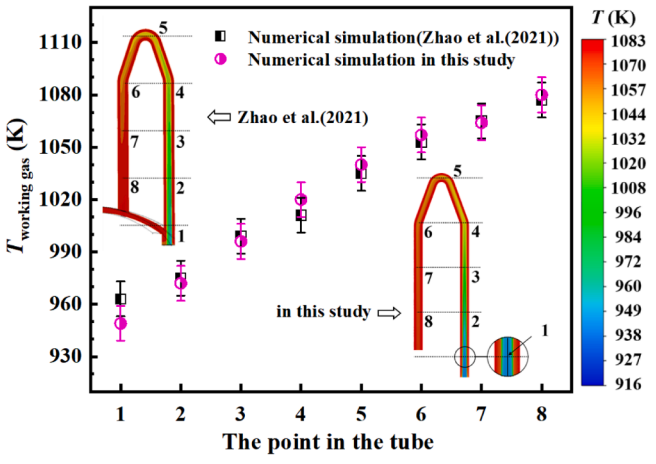

(b)

Fig. 4. Model validity verification of the heater: (a) with reference [43]; (b) with reference [34].

below 1.5 %. Thus, it was confirmed that the model implemented in the numerical simulation was reliable.

3. Results and discussion

3.1. Heat transfer characteristics in the heater

The heat transfer characteristics of the UTH and TTH were investigated under flue gas and working medium inlet flow rates of 1 m/s and 5 m/s, respectively, as tutorial examples. Fig. 5 shows the heat flux distribution on the heater tube wall. The highest heat flow density was observed in the top zone of the tube cluster, owing to the vertical flushing heating effect of the flue gas. The heat flow density of the outer tube cluster is considerably higher than that of the inner tube cluster. This is because the outer tube cluster was arranged less densely than the inner tube cluster, thus leading to sufficient accessibility to the flue gas to enhance heat transfer. The working medium flowed from the bottom of the outer tube cluster to the bottom of the inner tube cluster, whereas the flue gas flowed downward from the top of the heating chamber (shown in Fig. 1). This fluid flow mode caused a greater temperature difference between the working medium and the flue gas in the outer tube cluster than in the inner tube cluster. Additionally, the counter current heat exchange between the working medium and the flue gas in the outer tube cluster was more efficient than the down current heat exchange mode in the inner tube cluster. The heat flux on the TTH wall was higher than that on the UTH wall, particularly in the outer region (Fig. 5 (a) and 5 (b)). This is attributed to the increased cross-flushing velocity brought by the TTH, resulting in more adequate heat transfer. A lower working medium temperature was achieved in the outer tube cluster compared to that in the inner tube cluster; thus, the advantage of heat absorption was more obvious.

Flue gas was used as the external heat source for the heater. It flowed from the top to the bottom of the heating chamber. During this process, it flowed through the heating tube cluster and transferred heat to the working medium inside the heating tubes. For certain flus-gas inlet temperature and working-medium inlet temperatures, the heat absorbed by the working medium increased as the flus-gas outlet temperature decreased. Correspondingly, the outlet temperature of the working medium increased, and the work capacity was enhanced after entering the expansion chamber. Therefore, a lower flue gas outlet temperature and a higher working medium outlet temperature were preferred. Fig. 6 shows the temperatures of the flue gas outside the heating tube, tube wall, and the working medium inside the heating tube. The flue gas flushed the heating tube cluster from top to bottom, and the temperature gradually decreased, particularly in the contact zone with the tube cluster. Fig. 6 (a) shows the flue gas temperature cloud pattern at a cross-section of $x = 0$ mm. The blue low-temperature and green medium-temperature zones occur earlier in the TTH than in the UTH, and a larger blue low-temperature zone around the heating tube occurs in the TTH. Fig. 6 (a) also shows the flue gas temperature distribution cloud pattern at the cross sections of $y = 0$ mm and $y = 80$ mm. Compared with the UTH, the blue low-temperature zone was more pronounced near the heating-tube zone, whereas the temperature was more evenly distributed in the other zones of the y sections for the TTH. The above temperature distribution characteristics demonstrate that under the same inlet flue gas conditions, the flue gas temperature inside the TTH decreased significantly, and more heat was absorbed by the working medium inside the tube cluster.

The wall temperature distributions of the different heating tubes in the same cluster presented a similar tendency, and the wall temperature of the TTH was higher than that of the UTH (Fig. 6 (b)). The working medium temperature in the tube was similar to the tube wall temperature, and only a slight difference between the temperatures of the working medium and the wall was observed (shown in Fig. 6 (b) and Fig. 6 (c)). These findings illustrate that the heat transfer between the tube wall and the working medium inside the tube was more adequate

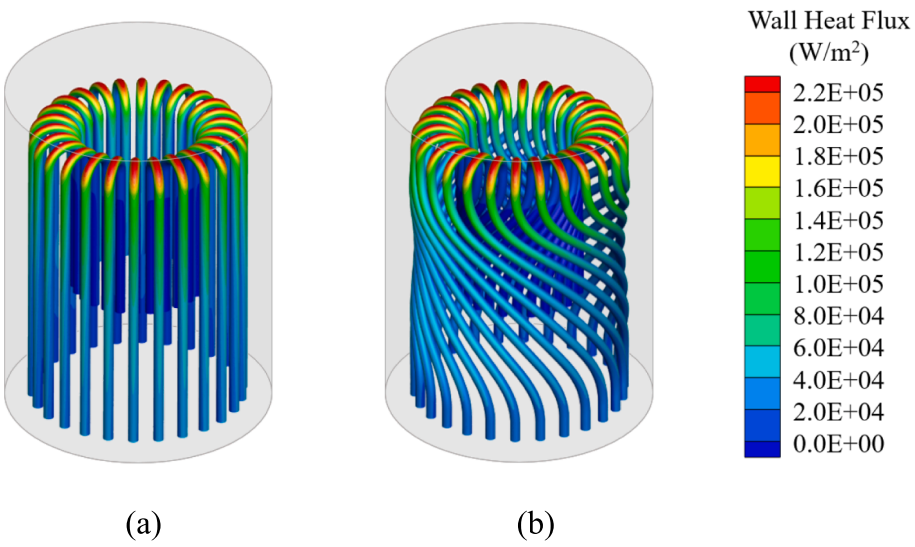

Fig. 5. Heat flux patterns in the wall of the heaters: (a)UTH; (b)TTH.

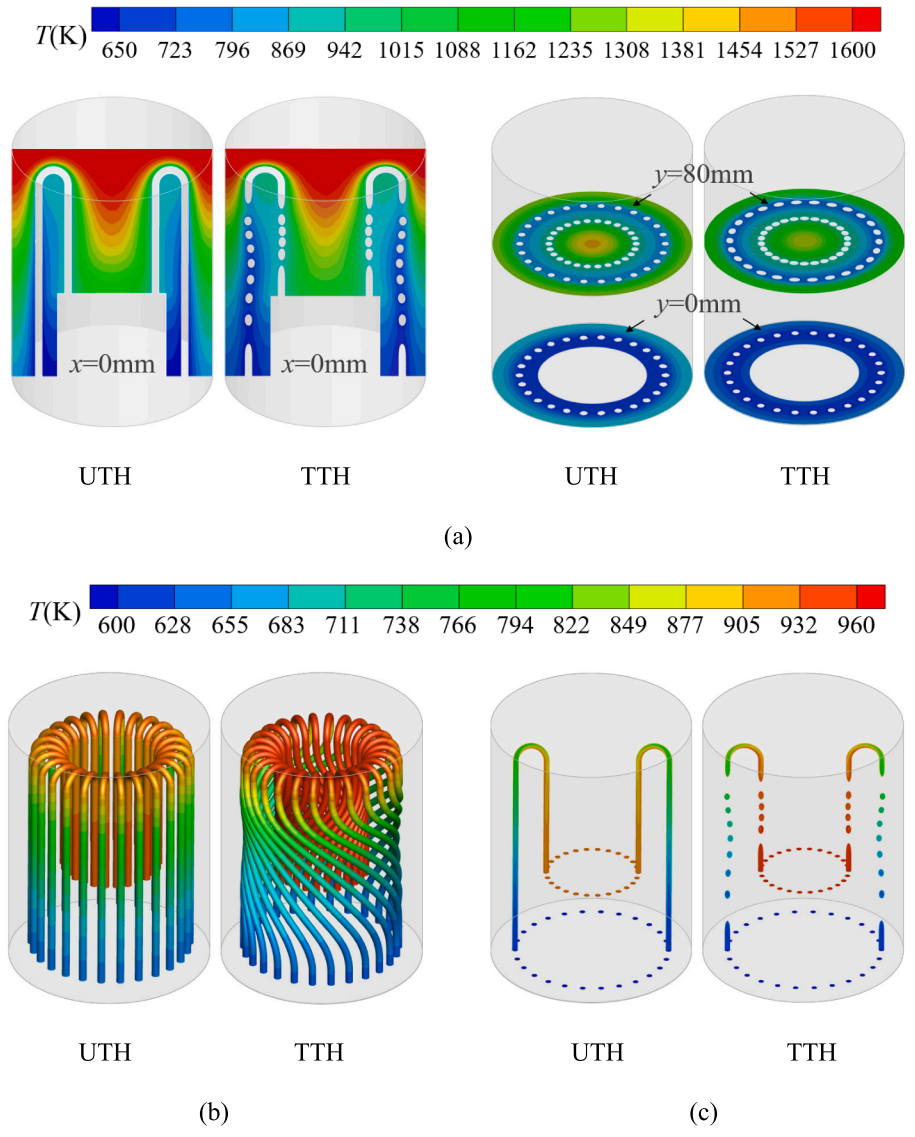

Fig. 6. Temperature cloud patterns of different parts: (a) the flue gas; (b) the wall; (c) the working medium.

than that between the flue gas and the tube wall. Furthermore, as shown in Fig. 6 (c), the working medium was gradually heated from the inlet to the outlet, resulting in a gradual increase in the temperature. The temperature increasement of the working medium in the TTH exceeded that in the UTH. This indicates that the working medium had a more robust working capacity for TTH after entering the expansion chamber.

3.2. Flow characteristics in the heater

The velocity distribution cloud patterns of UTH and TTH are shown in Fig. 7. The flue gas flow in the heating chamber was obstructed by the tube cluster and expansion chamber, as indicated by the velocity of the central axis cross section. The obstruction of flue gas flow was most significant at the top of the tube cluster bend and the top of the expansion chamber, in which a large low-velocity zone highlighted in dark blue was observed. Flue gas flow obstruction was also observed near the tube wall, except at the top of the tube cluster bend, which resulted in localized low-velocity zones near the tube wall. Compared with the UTH, the localized low-velocity zone was more evident in the TTH. Moreover, as shown by the flue gas velocity at the heating chamber outlet, the flue gas velocity in the inside region for the UTH was significantly lower than that in the outside region, whereas the flue gas velocity variation between the inside region and outside regions for the TTH was insignificant. This indicates that the TTH arrangement can improve the uniformity of the flue gas velocity at the radial cross section.

Compared to UTH, TTH provided a longer flow path for the fluid, especially for the working medium within the tube, which inevitably resulted in a higher pressure loss. An additional pressure loss of 0.2 Pa was achieved for the external flue gas in the TTH compared with that in the UTH, which was negligible in comparison with the overall pressure in the heater. As shown in Fig. 8, the pressure of the helium flow inside the tube was approximately 2 MPa. The pressure difference between the import and export of the working medium for the UTH was 458 Pa, whereas it was 646 Pa for TTH. The additional pressure consumption of 188 Pa is only 0.0094 % of the tube pressure. Therefore, compared with the total pressure inside the tube, the additional pressure loss caused by the TTH arrangement was minimal.

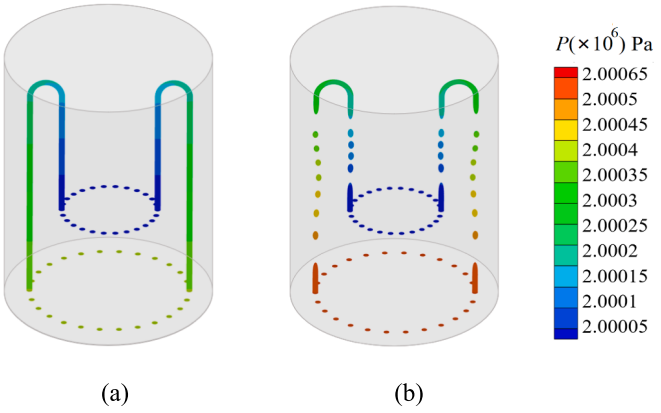

Fig. 8. Pressure cloud patterns of the working gas in heaters: (a)UTH; (b)TTH.

3.3. Effect of tube cluster torsional characteristics on the heat transfer performance of the heater

Fig. 9 shows that the outlet and inlet temperature differences of the working medium change regularly in the TTH under different inside and outside torsional angles (i.e. α and β). The inlet velocities of the working medium and flue gas were 15 and 3 m/s, respectively, in all cases. Fig. 9 (a) shows the results for the sum of the inside and outside torsional angles set at 180°, where the torsional angle of the outside tube exceeded that of the inside tube. The maximum outlet temperature of the working medium (893.7 K) was achieved at $\alpha = 140°$ and $\beta = 40°$. The temperature difference between the outlet and inlet was 293.7 K, and the rate of temperature increase was 48.95 % in this case. As the torsional angle of the outside tube increased, the working-medium temperature increase in the heating tube initially increased and then decreased. This observation can be attributed to two reasons. First, the increased length of the heating tube was more significant when the outside torsional angle was increased compared to the identical inside torsional angle, thus extending the heating path and time of the working medium in the heating tube. Second, the temperature of the working medium outside the tube increased to a greater extent than that inside the tube (Fig. 6 (c)). Thus, increasing the torsional angle of the outside tube was beneficial for increasing the overall working-medium temperature. The heat transfer in the outside tube was adequate when

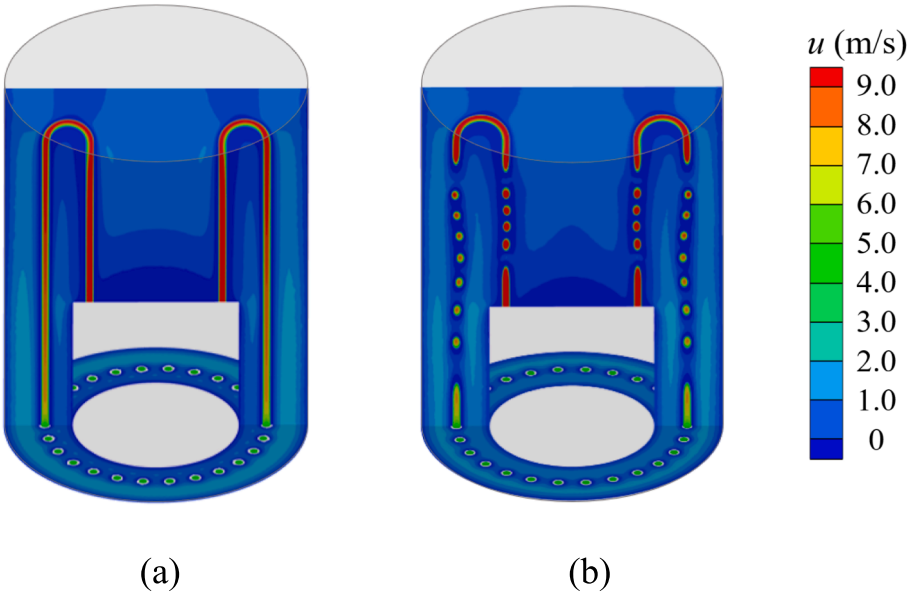

Fig. 7. Velocity cloud patterns of the heaters: (a)UTH; (b)TTH.

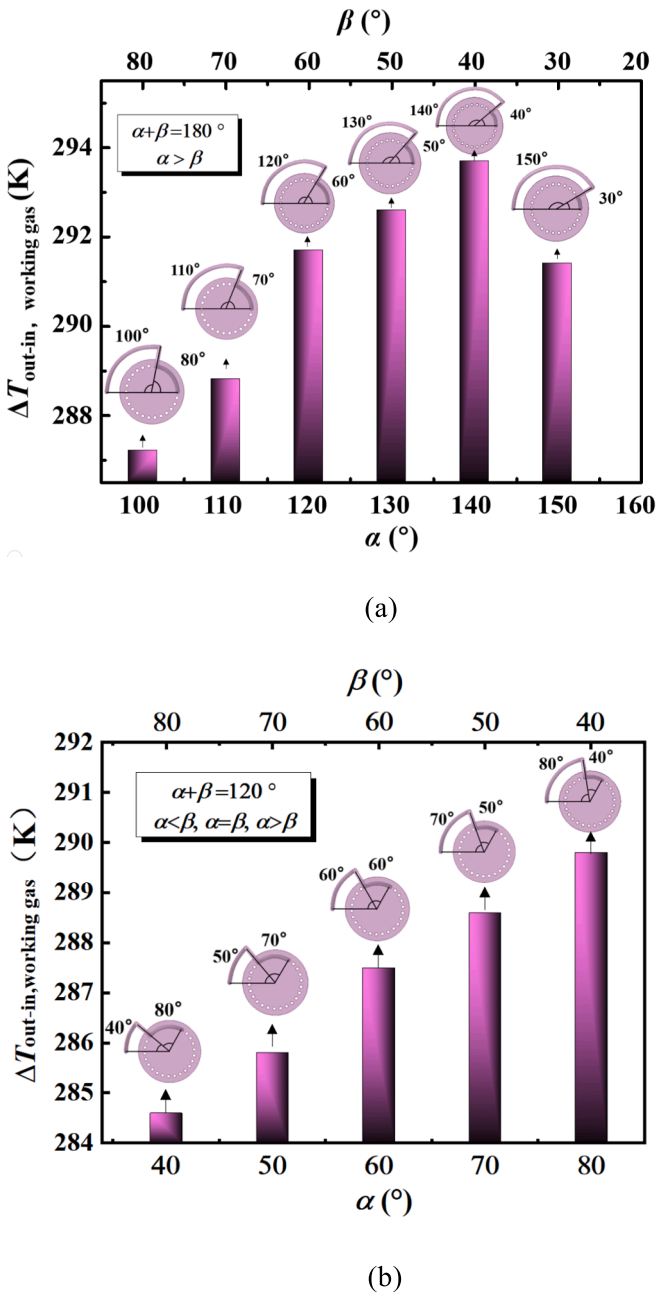

(a)

(b)

Fig. 9. Effect of torsional characteristics of tube cluster on heat transfer performance of heater: (a) $\alpha + \beta = 180°$, $\alpha > \beta$; (b) $\alpha + \beta = 120°$, $\alpha < \beta$, $\alpha = \beta$, $\alpha > \beta$.

achieving a certain point (e.g., $\alpha = 140°$, $\beta = 40°$). Beyond this critical point (e.g., $\alpha = 150°$, $\beta = 30°$), the inadequate heat transfer in the inside tube dominated the overall performance of the heater tube, and increasing α led to a reduction in the working medium outlet temperature. As shown in Fig. 9 (b), under the premise that the sum torsional angles of the inside and outside tubes are fixed at 120°, among the cases where the torsional angle of the outside tube is less than, equal to, and greater than the inside tube torsional angle, the former case is the most unfavourable to heat transfer, and the latter case is the most beneficial to heat transfer. Considering Fig. 9 (a) and (b), for the overall arrangement of the heating tubes, the outside tube torsional angle should exceed that of the inside tube and should be appropriately increased.

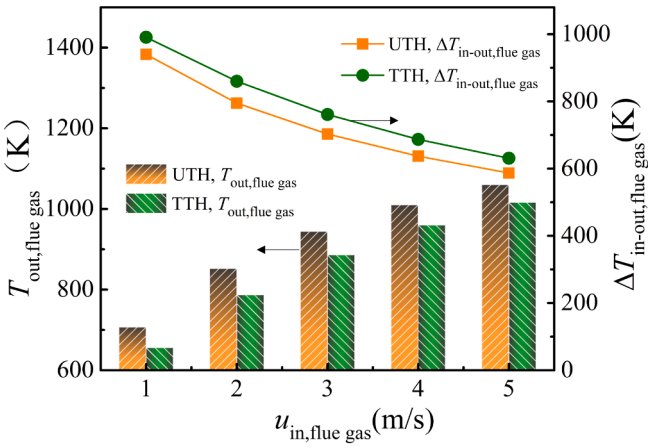

(a)

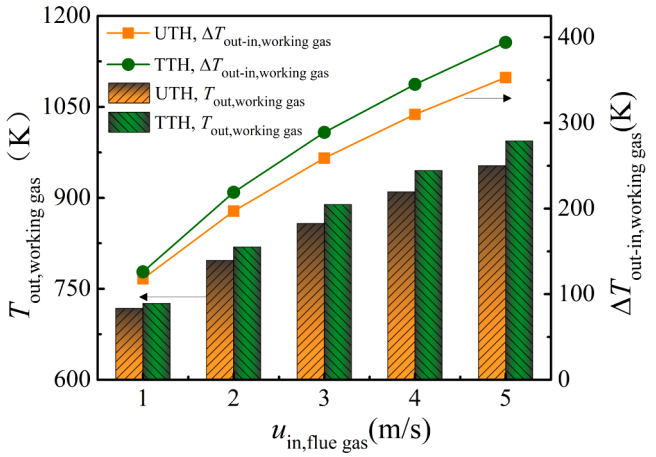

(b)

Fig. 10. Effect of flue gas inlet velocity on the heat transfer of the heaters: (a) the flue gas outlet; (b) the working gas outlet.

3.4. Effect of operating conditions on the heat transfer performance of the heater

3.4.1. Effect of flue gas inlet velocity

Fig. 10 shows the influence of the flue gas inlet velocity on the heat transfer performance of the heater; the working medium inlet velocity was set to 15 m/s as an example. When the flue gas velocity increased from 1 to 5 m/s, the temperature difference between the flue gas inlet and outlet for the UTH decreased from 940 to 587 K, with a maximum temperature decrease of 57.07 %, and the temperature difference between the flue gas inlet and outlet for the TTH decreased from 991 K to 631 K, with a maximum temperature decrease of 60.17 %. The larger the inlet flow velocity of the flue gas, the higher the outlet temperature of the flue gas, and the smaller the temperature difference between the flue gas inlet and outlet (shown in Fig. 10 (a)). This is because a higher flue gas flow rate results in a weaker cooling capacity per unit mass of flue gas in the working medium. Under the same flue-gas inlet velocity, the outlet temperature of the flue gas for the TTH was lower than that for the UTH, accompanied by a larger temperature difference between the flue-gas inlet and outlet. This indicated that the heat transfer performance of the TTH was superior to that of the UTH. Fig. 10 (b) shows the working-medium outlet temperature and the temperature rise from the inlet to the outlet under different flue-gas inlet velocities. When the flue gas velocity increases from 1 to 5 m/s, the temperature difference between

the working medium inlet and outlet for the UTH increases from 118 to 353 K, with a maximum temperature increase of 58.83 %. In contrast, the temperature difference between the working medium inlet and outlet for the TTH increases from 126 to 394 K, with a maximum temperature increase of 65.67 %. The higher the flue gas inlet velocity, the higher the working medium outlet temperature, and the larger the temperature rise of the working medium from the inlet to the outlet. This is because, for a larger flue gas inlet velocity, more heat is transferred to the working area per unit of time. For the same flue gas inlet velocity, the working medium outlet temperature of the TTH was higher than that of the UTH, and a larger temperature increase in the working medium from the inlet to the outlet was observed. Specifically, when the inlet velocity of the flue gas was 5 m/s, an additional temperature rise of 41 K for the working medium was obtained in the TTH compared with that in the UTH. Thus, the working ability of the working medium for the TTH was stronger.

3.4.2. *Effect of working medium inlet velocity*

The influence of the working-medium inlet velocity on the heat-exchange performance of the heater was investigated using a flue-gas inlet velocity of 3 m/s as an example; the results are shown in Fig. 11. When the working medium velocity increased from 5 to 25 m/s, the temperature difference between the flue gas inlet and outlet for the UTH increased from 567 to 731 K, with a maximum temperature decrease of 44.38 %, and the temperature difference between the flue gas inlet and outlet for the TTH increased from 595 to 797 K, with a maximum temperature decrease of 48.39 %. The greater the working-medium inlet velocity, the lower the outlet temperature of the flue gas, and the greater the temperature difference between the flue gas inlet and outlet (shown in Fig. 11 (a)). This is because, with an increase in the working-medium inlet velocity, the flue gas per unit mass was cooled more efficiently by the working medium. Under the same working-medium inlet velocity, the flue-gas temperature at the outlet of the TTH was lower than that at the UTH, accompanied by a larger temperature difference in the flue gas between the inlet and outlet. Thus, TTH achieved better heat exchange performance. With an increase in the inlet velocity of the working medium, the heat transfer enhancement of the TTH was more significant. For example, when the working-medium inlet velocity was 5 m/s, the flue-gas temperature drop from the inlet to the outlet for the TTH increased by 28 K than that for the UTH. Whereas it reached 66 K when the inlet velocity was 25 m/s. This indicated that more heat was transferred from the flue gas to the working medium inside the tube, thereby increasing the power capability of the Striling engine. Fig. 11 (b) shows that when the working-medium velocity increased from 5 to 25 m/s, the temperature difference between the working-medium inlet and outlet for the UTH decreased from 610 to 163 K, with a maximum temperature increase of 101.67 %, and the temperature difference between the working-medium inlet and outlet for the TTH decreased from 663 K to 182 K, with a maximum temperature increase of 110.5 %. The higher the inlet velocity, the lower the outlet temperature and the lower the temperature rise in the working medium. This is because the flue gas absorbs less heat per unit time at higher working medium velocities. Under the same working-medium inlet velocity, the working-medium outlet temperature of the TTH was higher than that of the UTH, accompanied by a higher temperature rise of the in working medium. For example, when the inlet velocity of the working medium was 5 m/s, the temperature of the working medium further increased by 53 K in the TTH compared with that in the UTH, thus enhancing the power capability of the working medium into the expansion chamber.

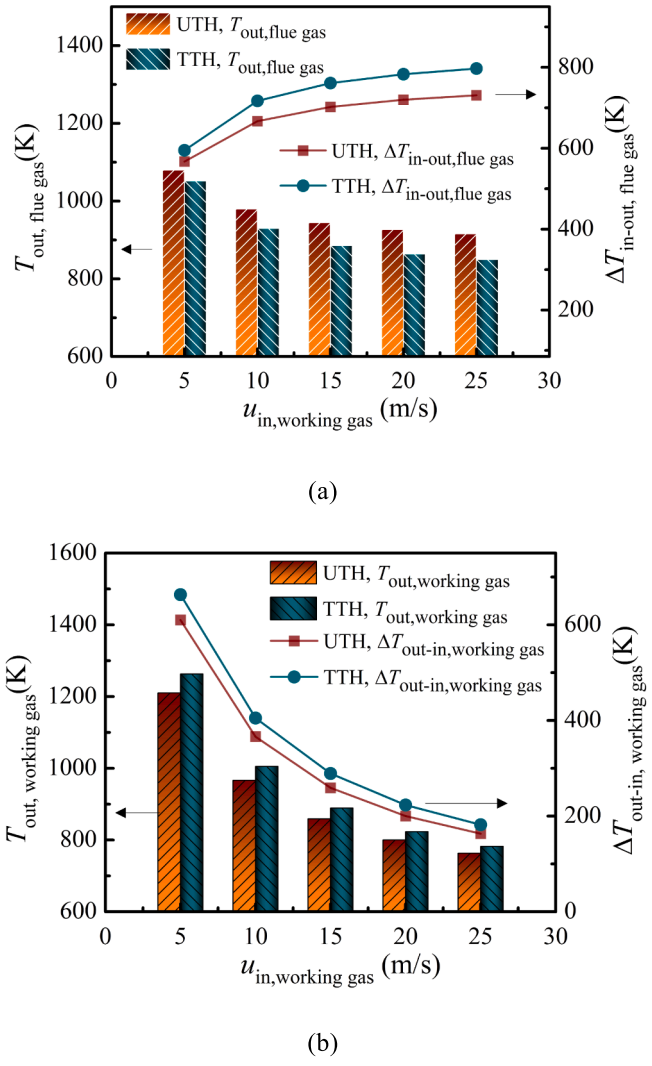

Fig. 11. Effect of working medium inlet velocity on the heat transfer performance of the heaters: (a) The flue gas outlet temperature and temperature drop; (b) The working gas outlet temperature and temperature rise.

The superiority of the TTH in terms of heat exchange is shown in Fig. 12. The heat-absorption capacity of the working medium at the TTH was significantly higher than that at the UTH. With an increase in the flue gas and working medium flow rates, the advantage of the TTH in terms of heat transfer was more significant. The heat absorption of the TTH increased by 183–910 J/s compared to that of the UTH within the range of working conditions in this study. In addition, the working-medium temperature rise ratio of TTH was increased by 6.5 %~12 % than that of UTH. With an increase in the flue gas flow rate, the working-

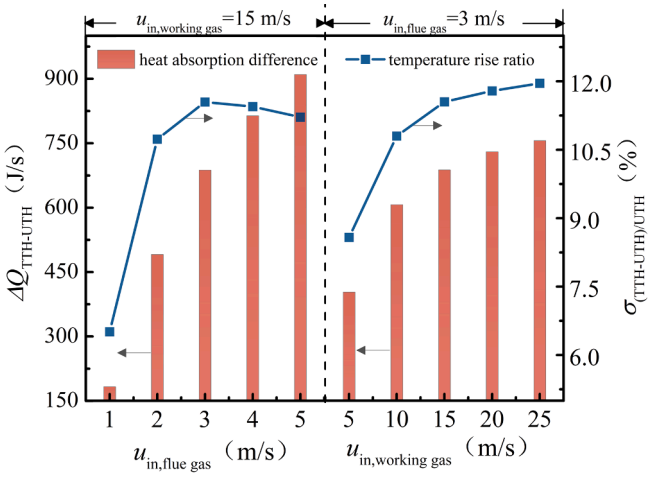

Fig. 12. Superiority of TTH over UTH in heat absorption and temperature rise ratio of working medium.

medium temperature rise ratio of TTH relative to UTH first increased and then decreased, whereas the temperature rise ratio of TTH relative to the UTH increased continuously as the working-medium flow rate increased.

3.4.3. *Effect of working medium kinds*

A Striling engine can use various gases such as H_2, He, N_2, air, Ar, and CO_2 as the working media. Fig. 13 shows the outlet temperature and pressure drop of the heater using different types of working medium for a flue gas inlet velocity of 3 m/s and working medium inlet velocity of 15 m/s. The maximum outlet temperature was obtained by using helium as the working medium. The outlet temperature of the working medium with helium were 859 K and 889 K for UTH and TTH, respectively. Compared with using other types of working media, the outlet temperature increase of TTH compared to UTH was the most notable when He was used as the working medium. The outlet temperature was primarily affected by the density and specific heat of the working medium, in which a greater density and specific heat were unfavourable for a temperature rise. The relative molecular mass of H_2, He, N_2, air, Ar, and CO_2 successively increased and the densities gradually increased. However, compared with the other working media, H_2 possessed a relatively large specific heat, whereas Ar possessed a small specific heat, thus displaying a non-monotonic decrease tendency for the outlet temperature, as shown in Fig. 13.

The pressure drop was mainly affected by the density and viscosity of the working medium; higher density and viscosity caused a more significant pressure drop. The relative molecular masses and densities of H_2, He, N_2, air, Ar, and CO_2 gradually increased, whereas Ar exhibited a relatively large viscosity. As a result, the pressure drop in the working medium also displayed a non-monotonically increasing tendency, as shown in Fig. 13. The pressure consumption of the working medium was the greatest when argon was used, whose pressure consumption was 5978 and 8627 Pa for UTH and TTH, respectively. The extra pressure consumption of the TTH compared to that of the UTH was the largest when argon was used as the working medium.

The outlet temperature of the working medium increased 10 ~ 30 °C when adopting TTH compared with UTH regardless of working medium kinds, accompanied by the increase of pressure drop of 227 ~ 1169 Pa, which was extremely small relative to the average system working pressure (2 MPa) in the heating tube. When considering the outlet temperature and pressure drop simultaneously, H_2 and He were superior in the TTH within the working range of this study.

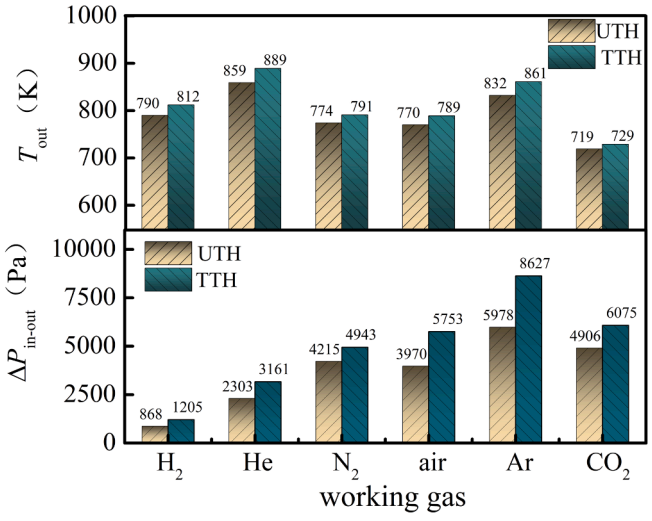

Fig. 13. Outlet temperature and pressure drop of the heater using different working medium.

4. Conclusions

In this study, a novel torsional tube cluster heater was designed to improve the heat transfer capacity of the heater, with the aim of increasing the actual operation efficiency of the Striling engine. Compared with a general U-shaped heater, the torsional tube cluster heater enhanced the lateral scouring velocity component of the flue gas towards the heating tubes, thus leading to more efficient heat transfer between the external heat source and the internal working medium. The main conclusions are as follows:

(1). The heat transfer enhancement characteristics of the torsional tube cluster heater were closely related to the torsional structural parameters. At a certain torsional angle, a better heat transfer capacity of the torsional tube cluster heater is achieved when the outside tube torsional angle exceeded the inside tube torsional angle. With an increase in the torsional angle of the outside tube, the working-medium outlet temperature in the heating tube first increased and then decreased for a certain total torsional angle. In this study, the maximum outlet temperature of the working medium (893.7 K) was achieved for outer tube circumferential torsional angles of 140° and inner tube circumferential torsional angles of 40°. The temperature difference between the outlet and inlet was 293.7 K, and the rate of temperature increase was 48.95 % in this case.

(2). The heat transfer enhancement characteristics of the torsional tube cluster heater were affected by the operating parameters. As the flue-gas inlet velocity increased, the temperature difference between the flue-gas inlet and outlet decreased, whereas that between the working-medium inlet and outlet increased. The maximum flue-gas temperature drops were 57.07 % and 60.17 %, and the maximum working-medium temperature increase were 58.83 % and 65.67 % for the UTH and TTH, respectively. As the inlet velocity of the working medium increased, the temperature difference between the flue gas inlet and outlet also increased. However, the temperature difference between the inlet and outlet of the working medium decreased. The maximum drops in the flue-gas temperature were 44.38 % and 48.39 %, and the maximum increases in the working-medium temperature were 101.67 % and 110.5 % for UTH and TTH, respectively. The temperature of the working medium at the outlet of the torsional tube cluster heater was 53 K higher than that of the U-shaped heater when the flue gas and working medium inlet velocities were was 3 and 5 m/s, respectively. An improvement in the outlet temperature of the working medium resulted in a higher work capacity in the expansion chamber.

(3). The heat transfer enhancement characteristics of the torsional tube cluster heater differed when different types of working media were used. Regardless of the type of working medium used, the outlet temperature of the working medium in the torsional tube cluster heater was higher than that of the U-shaped heater. The additional pressure loss caused by the torsional tube cluster heater was negligible relative to the system pressure (2 MPa). These results demonstrate the superiority of the torsional tube cluster heater in enhancing the heater heat transfer capacity, which is beneficial for improving the actual operational efficiency of the Striling engine.

CRediT authorship contribution statement

Feng Xin: Writing – review & editing, Writing – original draft, Visualization, Software, Methodology, Formal analysis, Conceptualization. **Kai Yang:** Visualization, Software, Methodology, Investigation. **Bin Zhao:** Writing – review & editing, Formal analysis, Conceptualization. **Yanfeng Yang:** Visualization, Software, Formal analysis. **Wei Liu:** Writing – review & editing, Validation, Formal analysis,

Conceptualization. **Zhichun Liu:** Writing – review & editing, Investigation, Formal analysis, Conceptualization.

Declaration of competing interest

The authors declare that they have no known competing financial interests or personal relationships that could have appeared to influence the work reported in this paper.

Data availability

Data will be made available on request.

Acknowledgements

This research was supported by the National Natural Science Foundation of China (52206069, 12304491), the Foundation of State Key Laboratory of Coal Combustion (FSKLCCA2310), the Doctoral Scientific Research Foundation of Changsha University of Science and Technology (000303910) and the Natural Science Foundation of Hunan Province, China (2020JJ5590)

Appendix A. Supplementary data

Supplementary data to this article can be found online at https://doi.org/10.1016/j.applthermaleng.2024.123334.

References

[1] H.S. Yang, H.Q. Zhu, X.Z. Xiao, Comparison of the dynamic characteristics and performance of beta-type Stirling engines operating with different driving mechanisms, Energy 275 (2023) 127535.
[2] M.A. Babazadeh, M. Babaelahi, M. Saadatfar, Enhancing solar stirling engine performance through the use of innovative heat transfer fin shapes, Int. J. Therm. Sci. 190 (2023) 108290.
[3] M.d. Al-Nimr, S.A. Khashan, H. Al-Oqla, Novel techniques to enhance the performance of Stirling engines integrated with solar systems Renew. Energ. 202 2023 894 906.
[4] K. Laazaar, N. Boutammachte, Development of a new technique of waste heat recovery in cement plants based on Stirling engine technology, Appl. Therm. Eng. 210 (2022) 118316.
[5] F. Catapano, C. Perozziello, B.M. Vaglieco, Heat transfer of a Stirling engine for waste heat recovery application from internal combustion engines, Appl. Therm. Eng. 198 (2021) 117492.
[6] D. Li, K. Qin, K. Luo, Underwater striling engine design with modified one-dimensional model, Int. J. Nav. Archit. Ocean Eng. 7 (2015) 526–539.
[7] Y. Qi, D. Sun, J. Zhang, Numerical study on a nuclear-powered Stirling system for space power generation, Appl. Therm. Eng. 233 (2023) 121140.
[8] E.F. de Moura, I.B. Henriques, G.B. Ribeiro, Thermodynamic-Dynamic coupling of a Stirling engine for space exploration, Therm. Sci. Eng. Prog. 32 (2022) 101320.
[9] G. Najafi, S.S. Hoseini, L.P.H. De Goey, T. Yusaf, Optimization of combustion in micro combined heat and power (mCHP) system with the biomass-Stirling engine using SiO2 and Al2O3 nanofluids, Appl. Therm. Eng. 169 (2020) 114936.
[10] J.W. Yang, W. Chen, B.W. Cao, X.H. Liu, H. Li, X.H. Li, D. Zhang, H.L. Zhang, Experimental investigation of the micro-power generation system based on porous burning, Appl. Therm. Eng. 234 (2023) 121205.
[11] F. Xin, Z. Liu, S. Wang, W. Liu, Study of heat transfer in oscillatory flow for a Stirling engine heating tube inserted with spiral spring, Appl. Therm. Eng. 143 (2018) 182–192.
[12] Z. Song, J. Chen, L. Yang, Heat transfer enhancement in tubular heater of Stirling engine for waste heat recovery from flue gas using steel wool, Appl. Therm. Eng. 87 (2015) 499–504.
[13] T. Kumaravelu, S. Saadon, A.R. Abu Talib, Heat transfer enhancement of a Stirling engine by using fins attachment in an energy recovery system, Energy 239 (2022) 121881.
[14] W. Ye, P. Yang, Y. Liu, Multi-objective thermodynamic optimization of a free piston Stirling engine using response surface methodology, Energy Convers. Manag. 176 (2018) 147–163.
[15] R. Wang, J. Hu, Z. Jia, E. Luo, J. Xu, Y. Sun, Performance study of a free-piston Stirling heat pump with a circumferential temperature gradient in the heating heat exchanger, Int. J. Refrig. 146 (2023) 274–289.
[16] N. Regalado-Rodríguez C. Militello Comparative study of the effects of increasing heat transfer area within compression and expansion chambers in combination with modified pistons in Stirling engines. A simulation approach based on CFD and a numerical thermodynamic model Energy Convers. Manag. 268 (2022) 115930.
[17] K.M. Bataineh, M.F. Maqableh, A new numerical thermodynamic model for a beta-type Stirling engine with a rhombic drive, Therm. Sci. Eng. pro. 28 (2022) 101071.
[18] L. Kuban, J. Stempka, A. Tyliszczak, A 3D-CFD study of a γ-type Stirling engine, Energy 169 (2019) 142–159.
[19] D.-J. Kim, Y. Park, T.Y. Kim, K. Sim, Design optimization of tubular heat exchangers for a free-piston Stirling engine based on improved quasi-steady flow thermodynamic model predictions, Energies 15 (2022) 3326.
[20] F. Ahmed, S. Zhu, G. Yu, E. Luo, A potent numerical model coupled with multi-objective NSGA-II algorithm for the optimal design of Stirling engine, Energy 247 (2022) 123468.
[21] H.-S. Yang M. Aon Ali K. Venkata Ravi Teja, Y.-F. Yen, Parametric study and design optimization of a kW-class beta-type Stirling engine Appl. Therm. Eng. 215 (2022) 119010.
[22] A.A. El-Ehwany, G.M. Hennes, E.I. Eid, E. El-Kenany, Experimental investigation of the performance of an elbow-bend type heat exchanger with a water tube bank used as a heater or cooler in alpha-type Stirling machines, Renew, Energ. 36 (2011) 488–497.
[23] G. Xiao, U. Sultan, M. Ni, H. Peng, X. Zhou, S. Wang, Z. Luo, Design optimization with computational fluid dynamic analysis of β-type Stirling engine, Appl. Therm. Eng. 113 (2017) 87–102.
[24] W. Liu, P. Liu, J.B. Wang, N.B. Zheng, Z.C. Liu, Exergy destruction minimization: A principle to convective heat transfer enhancement, Int. J. Heat Mass Transf. 122 (2018) 11–21.
[25] W. Liu, P. Liu, Z.M. Dong, K. Yang, Z.C. Liu, A study on the multi-field synergy principle of convective heat and mass transfer enhancement, Int. J. Heat Mass Transf. 134 (2019) 722–734.
[26] L. Liu, T. Sun, Y. Cao, X. Yu, L. Zhang, Z. Cao, L. Zhang, W. Xu, S. Bu, Experimental and numerical investigation on the flow and heat transfer characteristics of the tube with an integrated internal longitudinal fin, Int. J. Therm. Sci. 183 (2023) 107857.
[27] L. Solomon, S. Qiu, Computational analysis of external heat transfer for a tubular Stirling convertor, Appl. Therm. Eng. 137 (2018) 134–141.
[28] F. Xin, Z. Liu, N. Zheng, P. Liu, W. Liu, Numerical study on flow characteristics and heat transfer enhancement of oscillatory flow in a spirally corrugated tube, Int. J. Heat Mass Transf. 127 (2018) 402–413.
[29] N. Hirao, M. Komura, Improvement in specific power of Stirling engine by using a new heat exchanger, J. Jpn. Inst. Energy 88 (2009) 1095–1100.
[30] A.A. El-Ehwany, G.M. Hennes, E.I. Eid, E.A. El-Kenany, Development of the performance of an alpha-type heat engine by using elbow-bend transposed-fluids heat exchanger as a heater and a cooler, Energy Convers. Manag. 52 (2011) 1010–1019.
[31] A.C. Ferreira, M.L. Nunes, J.C.F. Teixeira, L.A.S.B. Martins, S.F.C.F. Teixeira, Thermodynamic and economic optimization of a solar-powered Stirling engine for micro-cogeneration purposes, Energy 111 (2016) 1–17.
[32] S. Islas, R. Beltran-Chacon, N. Velázquez, D. Leal-Chávez, R. López-Zavala, J. A. Aguilar-Jiménez, A numerical study of the influence of design variable interactions on the performance of a Stirling engine System, Appl. Therm. Eng. 170 (2020) 115039.
[33] S. Zhu, G. Yu, K. Liang, W. Dai, E. Luo, A review of Stirling-engine-based combined heat and power technology, Appl. Energy 294 (2021) 116965.
[34] W. Zhao, R. Li, H. Li, Y. Zhang, S. Qiu, Numerical analysis of fluid dynamics and thermodynamics in a stirling engine, Appl. Therm. Eng. 189 (2021) 116727.
[35] C.-Y. Wu, G.M.D. Currao, W.-L. Chen, C.-Y. Chang, B.-Y. Hu, T.-H. Wang, Y.-C. Chen, The application of an innovative integrated Swiss-roll-combustor/Stirling-hot-end component on an unpressurized Stirling engine, Energy Convers. Manag. 249 (2021) 114831.
[36] Z. Jiang, G. Yu, S. Zhu, W. Dai, E. Luo, Advances on a free-piston Stirling engine-based micro-combined heat and power system, Appl. Therm. Eng. 217 (2022) 119187.
[37] E. Cardozo, A. Malmquist, Performance comparison between the use of wood and sugarcane bagasse pellets in a Stirling engine micro-CHP system, Appl. Therm. Eng. 159 (2019) 113945.
[38] S.A. El-Ghafour, M. El-Ghandour, N.N. Mikhael, Three-dimensional computational fluid dynamics simulation of stirling engine, Energy Convers. Manag. 180 (2019) 533–549.
[39] R. Gheith, H. Hachem, F. Aloui, S., Ben Nasrallah, Experimental and theoretical investigation of Stirling engine heater: Parametrical optimization, Energy Convers. Manag. 105 (2015) 285–293.
[40] G. Xiao, C. Chen, B. Shi, K. Cen, M. Ni, Experimental study on heat transfer of oscillating flow of a tubular Stirling engine heater, Int. J. Heat Mass Transf. 71 (2014) 1–7.
[41] M. Ni, B. Shi, G. Xiao, Z. Luo, K. Cen, Heat transfer characteristics of the oscillating flows of different working gases in U-shaped tubes of a Stirling engine, Appl. Therm. Eng. 89 (2015) 569–577.
[42] J.X. Li, Design and research of the heater for the small scale Stirling engine [Master], Dailian University of technology, 2012.
[43] C.-H. Cheng, Y.-F. Chen, Numerical simulation of thermal and flow fields inside a 1-kW beta-type Stirling engine, Appl. Therm. Eng. 121 (2017) 554–561.